Application of Improved Recursive Integral Perfect Matched Layer Method on Ultrasonic Testing

Dong Wei, Xue Zhao, Jing Wang, and Jie-Sheng Wang

Abstract—**In-suit ultrasonic testing of the inner surface of welded pipe is necessary for continuous production, because multiple sorts of burr may exist in the surface after scraping treatment. The regular extent of weld shape has a great influence on the detection signal, analyzing the variation of signal characteristic caused by various burrs has great significance to the actual testing. The split perfect matched layer method is introduced in finite difference of time domain method. Frequency shift extension function is used to decrease the boundary reflection in the perfect matched layer, and cosine type attenuation function is adopted. Recursive integral method in the sound field is implemented to cut off the boundary, which can reduce the system memory requirements. Simulation calculations were complemented to analyze the absorption of the recursive integral perfect matched layer method. Inner burr simulation model is constructed to analyze the signal characteristic of various burrs. Inner burr detecting system is established with sprayed water-coupled line focused probe. Experiment results of electric resistance welded steel pipe sample coincide with numerical simulation results very well, that verify the effectiveness of analysis conclusion.**

Index Terms—**recursive integral, perfect matched layer, finite difference time domain method, welded pipe inner burr**

I. Introduction

THE transportation process of Oil and gas usually requires that pipeline have many advantages, for example, collapsing capacity, low cost etc. A variety of welded steel pipes have been widely used in petroleum and natural gas transmission. Currently, physical dimension and surface quality of the pipe have become increasingly demanding. Multiple sorts of burrs [1] existing in the production process of weld pipe surface treatment, due to the scraper blade and the problem of height control. Outer burr detection is more intuitive and easily to be determined by artificial method or video image processing method, but the inner burr within the pipe wall cannot be directly observed. Ultrasonic testing method is suitable to discriminate various burrs. Based on this we proposed a method for detecting and discriminating welded pipe inner burr. Depending on the characteristics of the inner burr, using water coupled line focus method and making the focal spot area parallel to the weld pipe for detecting the distribution of the wall thickness of the inner pipe. Discrimination of the inner burr can be achieved.

Detecting the inside wall shape of welded pipe is to be realized the basis of inner burr detection. The analysis and evaluation of ultrasonic testing signal results of the inner burr is more difficult, because of the material properties of the weld, irregular boundary characteristics caused by the inner burr, similar to the theoretical research is also relatively rare. Finite difference method is widely applied to the analysis of elastic waves, it can be well analyzed ultrasonic wave propagation condition and echo signal under the action of defects [2], and preliminary research results also demonstrate the effectiveness of this method. Sound field variables are divided by boundary absorption method, more space can be truncated for numerical simulation, and artificial truncation boundary without reflection is the key to process successful numerical simulation. In the elastic wave finite difference simulation, PML is the most widely used method and is known as the best-absorbed boundary absorbing conditions. PML was originally proposed by BERENGER to resolve the border issue of electromagnetic fields [3]. PML boundary absorbing have been studied and improved by many researchers. The stability of the boundary absorption were analyzed by M.N. Dmitriev and V.V. Lisitsa [4] , a necessary condition of boundary absorbing stability is obtained by enlarging the phase velocity into the Taylor series. Fang Dagang [5] decomposed a sparse matrix which generate from FDTD with weighted Lagrangian polynomial into two three-diagonal matrices, eliminating the constraints of stability conditions and improving the computing speed. In addition, the conventional finite difference method exist many disadvantages, which can affect the efficiency of numerical simulation analysis, such as it takes up more

Manuscript received September 9, 2016; revised December 26, 2016. This work was supported by the Project by National Natural Science Foundation of China (Grant No. 21576127), the Program for Liaoning Excellent Talents in University (Grant No. LR2014008), the Project by Liaoning Provincial Natural Science Foundation of China (Grant No. 2014020177), the Program for Research Special Foundation of University of Science and Technology of Liaoning (Grant No. 2015TD04) and the Opening Project of National Financial Security and System Equipment Engineering Research Center (Grant No. USTLKFGJ201502 and USTLKEC201401).

Dong Wei is with the School of Electronic and Information Engineering, University of Science and Technology Liaoning, Anshan, 114051, PR China. (phone: 86-0412-5929747; e-mail: asweidong@126.com).

Xue Zhao is a postgraduate student in the School of Electronic and Information Engineering, University of Science and Technology Liaoning, Anshan, 114051, PR China. (e-mail: zx992992@126.com).

Jing Wang is a postgraduate student in the School of Electronic and Information Engineering, University of Science and Technology Liaoning, Anshan, 114051, PR China. (e-mail: aswangjing@163.com).

Jie-Sheng Wang is with the School of Electronic and Information Engineering, University of Science and Technology Liaoning, Anshan, 114051, PR China; National Financial Security and System Equipment Engineering Research Center, University of Science and Technology Liaoning. (phone: 86-0412-2538246; fax: 86-0412-2538244; e-mail: wang_jiesheng@126.com).

memory and have a long running time when the boundary absorption process. Some scholars have conducted a special research [6] to solve this problem. But the conventional finite difference method mainly used for analysis in electromagnetic field [7], the application of ultrasonic field is still very rare.

The ultrasonic field analysis is complemented by the RIPML (Recursive Integral Perfect Matched Layer) method to improve the usefulness of the numerical simulation. Finally, numerical simulation experiments on the inner burr of welded pipe and through practical testing to verify the feasibility and effectiveness of this method.

II. Split PML method and improvement

FDTD (Finite Difference Time domain) method needs boundary absorb to truncate the infinite space for conducting numerical simulation. Fixed grid spacing is adopted by the traditional finite difference algorithms to the entire model domain, a smaller sampling step must be used to the whole region in order to obtain accurate simulation results, which need more computation and memory [7]. SPML (Splitting PML) is simple, but need a large storage capacity; otherwise, NPML (Non-splitting PML) method do not need the dividing of the Field components, but need a large number of convolution calculation in the time domain, which make the equation more complex and produce a large of calculation. In order to improve the NPML, reduce memory space and enhance computing speed, integral calculation is introduced in this paper based on the FDTD method.

A. Finite difference model of SPML

According to splitting ideology of BERENGER [3], field component will be broken down into two parts, the two-dimensional sound field equations as follows:

$$\begin{cases} \frac{\partial v_x^{\ x}}{\partial t}+d(x)v_x^{\ x}=\frac{1}{\rho}\frac{\partial \tau_{xx}}{\partial x} \\ \frac{\partial v_x^{\ z}}{\partial t}+d(x)v_x^{\ z}=\frac{1}{\rho}\frac{\partial \tau_{xz}}{\partial z} \\ \frac{\partial v_z^{\ x}}{\partial t}+d(x)v_z^{\ x}=\frac{1}{\rho}\frac{\partial \tau_{xz}}{\partial x} \\ \frac{\partial v_z^{\ z}}{\partial t}+d(z)v_z^{\ z}=\frac{1}{\rho}\frac{\partial \tau_{zz}}{\partial z} \\ \frac{\partial \tau_{xx}^{\ z}}{\partial t}+d(x)\tau_{xx}^{\ z}=(\lambda+2\mu)\frac{\partial v_x}{\partial z} \\ \frac{\partial \tau_{xx}^{\ z}}{\partial t}+d(z)\tau_{xx}^{\ z}=\lambda\frac{\partial v_z}{\partial z} \\ \frac{\partial \tau_{xz}^{\ x}}{\partial t}+d(x)\tau_{xz}^{\ x}=\mu\frac{\partial v_z}{\partial x} \\ \frac{\partial \tau_{xz}^{\ z}}{\partial t}+d(z)\tau_{xz}^{\ z}=\mu\frac{\partial v_x}{\partial z} \\ \frac{\partial \tau_{zz}^{\ x}}{\partial t}+d(x)\tau_{zz}^{\ x}=\lambda\frac{\partial v_x}{\partial x} \\ \frac{\partial \tau_{zz}^{\ z}}{\partial t}+d(z)\tau_{zz}^{\ z}=(\lambda+2\mu)\frac{\partial v_z}{\partial z} \end{cases} \tag{1}$$

where λ and μ are the Lame coefficients, v is the particle velocity, τ is the stress, $d(x)$ and $d(z)$ are the attenuation factors.

B. Model improvement

In the electromagnetic field, frequency shift extension function is introduced into PML to reduce the boundary reflection by Roden and Gedney [9]. First order speed-stress equations are transmitted to stretching coordinate domain by extension function. In the frequency domain, the two-dimensional extension functions of x and y planes [10] can be written as:

$$\begin{cases} \varepsilon_x=k_x+\frac{d(x)}{\alpha_x+i\omega} \\ \varepsilon_z=k_z+\frac{d(z)}{\alpha_z+i\omega} \end{cases} \tag{2}$$

where k and α are auxiliary attenuation factors, which $k\geq 1$, $\alpha\geq 1$.

In the stretching coordinates, the space differential of PML space is written as:

$$\begin{cases} \frac{\partial}{\partial \tilde{x}}\Rightarrow\frac{1}{\varepsilon_x}\frac{\partial}{\partial x} \\ \frac{\partial}{\partial \tilde{z}}\Rightarrow\frac{1}{\varepsilon_z}\frac{\partial}{\partial z} \end{cases} \tag{3}$$

According to Eq. (3), auxiliary variable stress tensor S and the strain rate tensor E are introduced. In the stretching coordinates, first order speed-stress equations can be written as:

$$\begin{cases} \frac{\partial v_x}{\partial t}=\frac{1}{\rho}(S_{xx}+S_{xz}) \\ \frac{\partial v_z}{\partial t}=\frac{1}{\rho}(S_{zx}+S_{zz}) \\ \frac{\partial \tau_{xx}}{\partial t}=(\lambda+2\mu)E_{xx}+\lambda E_{zz} \\ \frac{\partial \tau_{xz}}{\partial t}=\mu(E_{zx}+E_{xz}) \\ \frac{\partial \tau_{zz}}{\partial t}=(\lambda+2\mu)E_{zz}+\lambda E_{xx} \end{cases} \tag{4}$$

To introduce the stress tensor S and the strain rate tensor E, the speed stress field is no longer doing the split of field components, thus saving memory. The iterative formulas of the stress tensor are given by Eq. (5):

$$\begin{cases} S^n_{\ xx}=\xi_x(\frac{\partial \tau^n_{\ xx}}{\partial x}-\frac{\Delta t}{1+0.5\Delta t}\Omega^{n-1}_{\ xx}) \\ S^n_{\ xz}=\xi_z(\frac{\partial \tau^n_{\ xz}}{\partial z}-\frac{\Delta t}{1+0.5\Delta t}\Omega^{n-1}_{\ xz} \\ S^n_{\ zx}=\xi_x(\frac{\partial \tau^n_{\ xz}}{\partial x}-\frac{\Delta t}{1+0.5\Delta t}\Omega^{n-1}_{\ zx}) \\ S^n_{\ zz}=\xi_z(\frac{\partial \tau^n_{\ zz}}{\partial z}-\frac{\Delta t}{1+0.5\Delta t}\Omega^{n-1}_{\ zz}) \end{cases} \tag{5}$$

In the Eq (5), n is discrete time, Ω is the sum of stress

tensors. Iterative calculation equations of Ω as follows:

$$\begin{cases} \Omega^{n}{}_{xx} = \Omega^{n-1}{}_{xx} + (d(x)+\alpha_x k_x)S^{n}{}_{xx} - \alpha_x \dfrac{\partial \tau_{xy}}{\partial x} \\ \Omega^{n}{}_{xz} = \Omega^{n-1}{}_{xz} + (d(x)+\alpha_x k_x)S^{n}{}_{xz} - \alpha_z \dfrac{\partial \tau_{xz}}{\partial z} \\ \Omega^{n}{}_{zx} = \Omega^{n-1}{}_{zx} + (d(z)+\alpha_z k_z)S^{n}{}_{zx} - \alpha_x \dfrac{\partial \tau_{zx}}{\partial x} \\ \Omega^{n}{}_{zz} = \Omega^{n-1}{}_{zz} + (d(z)+\alpha_z k_z)S^{n}{}_{zz} - \alpha_z \dfrac{\partial \tau_{zz}}{\partial z} \end{cases} \tag{6}$$

Multiplication factors ζ_x and ζ_z are defined as:

$$\begin{cases} \xi_x = \dfrac{1+0.5\Delta t\alpha_x}{0.5\Delta t(d(x)+\alpha_x k_x)+k_x} \\ \xi_z = \dfrac{1+0.5\Delta t\alpha_z}{0.5\Delta t(d(z)+\alpha_z k_z)+k_z} \end{cases} \tag{7}$$

In the same way, a series of similar equations of the strain rate tensor are acquired. Combined with Eq.(4)-(7), differential formulas can be obtained as Eq. (8):

$$\begin{cases} v_x(t+\frac{\Delta t}{2}) = v_x(t-\frac{\Delta t}{2}) + \frac{\Delta t}{\rho}(S_{xx}+S_{xz}) \\ \quad + \frac{\Delta t^3}{24\rho^2}[(\lambda+2\mu)(\frac{\partial^2 S_{xx}}{\partial x^2}+\frac{\partial^2 S_{xz}}{\partial x^2}) \\ \quad + (\lambda+\mu)(\frac{\partial^2 S_{zx}}{\partial x\partial z}+\frac{\partial^2 S_{zz}}{\partial x\partial z}) + \mu(\frac{\partial^2 S_{xx}}{\partial z^2}+\frac{\partial^2 S_{xz}}{\partial z^2})] \\ v_z(t+\frac{\Delta t}{2}) = v_z(t-\frac{\Delta t}{2}) + \frac{\Delta t}{\rho}(S_{zx}+S_{zz}) \\ \quad + \frac{\Delta t^3}{24\rho^2}[\mu(\frac{\partial^2 S_{zx}}{\partial x^2}+\frac{\partial^2 S_{zz}}{\partial x^2}) + (\lambda+\mu)(\frac{\partial^2 S_{xx}}{\partial x\partial z}+\frac{\partial^2 S_{xz}}{\partial x\partial z}) \\ \quad + (\lambda+2\mu)(\frac{\partial^2 S_{zx}}{\partial z^2}+\frac{\partial^2 S_{zz}}{\partial z^2})] \\ \tau_{xx}(t+\Delta t) = \tau_{xx}(t) + \Delta t(\lambda+2\mu)(E_{xx}+E_{zz}) \\ \quad + \frac{\Delta t^3}{24\rho}[(\lambda+2\mu)((\lambda+2\mu)\frac{\partial^2 E_{xx}}{\partial x^2}+\lambda\frac{\partial^2 E_{zz}}{\partial x^2}) \\ \quad + 2\mu(\lambda+\mu)(\frac{\partial^2 E_{zx}}{\partial x\partial z}+\frac{\partial^2 E_{xz}}{\partial x\partial z}) \\ \quad + \lambda((\lambda+2\mu)\frac{\partial^2 E_{zz}}{\partial z^2}+\lambda\frac{\partial^2 E_{xx}}{\partial z^2})] \\ \tau_{zz}(t+\Delta t) = \tau_{zz}(t) + \Delta t((\lambda+2\mu)E_{zz}+\lambda E_{xx}) \\ \quad + \frac{\Delta t^3}{24\rho}[\lambda((\lambda+2\mu)\frac{\partial^2 E_{xx}}{\partial x^2}+\lambda\frac{\partial^2 E_{zz}}{\partial x^2}) \\ \quad + 2\mu(\lambda+\mu)(\frac{\partial^2 E_{zx}}{\partial x\partial z}+\frac{\partial^2 E_{xz}}{\partial x\partial z}) \\ \quad + (\lambda+2\mu)((\lambda+2\mu)\frac{\partial^2 E_{zz}}{\partial z^2}+\lambda\frac{\partial^2 E_{xx}}{\partial z^2})] \\ \tau_{xz}(t+\Delta t) = \tau_{xz}(t) + \Delta t\mu(E_{zx}+E_{xz}) + \frac{\Delta t^3}{24\rho}\mu[\mu(\frac{\partial^2 E_{zx}}{\partial x^2}+\lambda\frac{\partial^2 E_{xz}}{\partial x^2}) \\ \quad + 2(\lambda+\mu)(\frac{\partial^2 E_{xx}}{\partial x\partial z}+\frac{\partial^2 E_{zz}}{\partial z^2}) + \mu(\frac{\partial^2 E_{zx}}{\partial z^2}+\frac{\partial^2 E_{xz}}{\partial z^2}) \end{cases} \tag{8}$$

C. Selection of attenuation factors

Attenuation factors were analyzed by many researchers in the boundary absorption. An attenuation function about an index relationship between truncated border by the within domain and the interface distance of PML is proposed by Collino [11] etc. This method has been obtained a widely application in the boundary absorption. Chen Keyang [12] suggested to use a cosine-type attenuation function, that the attenuation factors along with the sine and cosine function, increasing speed slower along the outside of model, the better absorption boundary. These attenuation functions are analyzed by Gao Gang [13] and others, and verifying the simulation results of wave field of cosine-type attenuation factors better than other attenuation factor. In this paper, a cosine-type attenuation function is employed as follows:

$$d(x) = 0.5 + 0.5\cos(\beta x\pi / L) \tag{9}$$

where, the empirical value of β is 1, x is the attenuation distance, range of x is from 0 to L, L is the thickness of PML.

III. RIPML Contrast Algorithms

A. Comparison of algorithm possession resources

There are two PML methods can effectively absorb layman waves on the simulation results, it is difficult to distinguish the difference of them. Although the process has two different algorithms, that can achieve the same accuracy and performance [14]. However, there is a large difference in the amount of computation. Updating the value of the stress tensor do not need to store the value of its previous time, the value of the strain rate tensor is also the case. Therefore, do not need to distribute additional memory space for them. Auxiliary variables only have the sum of the stress tensor and the sum of the strain rate tensor of the recursive calculation, which need to be stored in the computer memory. In the two-dimensional model, absorbing boundary region is divided into corners and edges in order to save memory.

In some areas of the model, the value of attenuation factor is zero, which lead to the value of the sum of the stress tensor and the sum of the strain rate tensor are zero, so that do not need to consider these variables. Comparing to the minimum number of variables of the two algorithms, SPML algorithm requires storage field components, the minimum number of variables which require to store in the improved RIPML have a slight increase in the corner area, while there is a decrease in the edge region. In most cases, compared to the region of the edge, the corner area is much smaller, on the whole, the improved algorithm takes up less memory, and calculation amount is reduced accordingly.

B. Calculation of gas-liquid-solid coupling interface

The calculation model using the ideal model of gas-liquid-solid coupling interface shown in Figure 1, three quarters of the upper part is water, steel existing in the $1/12$ of the lower part, $1/6$ is the air. Which the density of water is $\rho = 1g/cm^3$, the velocity of longitudinal wave and transverse wave are taken as $v_p = v_s = 1500m/s$, the density of steel is $7.85g/cm^3$, the velocity of longitudinal wave is taken as $v_p = 5850m/s$, the speed of shear wave is taken as $v_s = 3230m/s$, the height of the whole calculation model is $60mm$. Calculation parameters as follows: space distance is $0.05mm$, time interval is $1ns$, the position of the incentive point at $15mm$ on the top of the liquid-solid interface, the diameter of probe is $10mm$, using $5MHz$ sinusoidal

excitation of 5 cycles, the thickness of PML layer is $10\Delta x$.

The stress distribution of numerical simulation is shown in Figure 2. Seen from the calculation results, RIPML has a good absorption effect; numerical calculation can be operated correctly. The simulation of ultrasonic flaw detection to be treated in the range of the model width from $13mm$ to $22mm$, using single transmitter and single receiver probes, through the average of each point of the echo signal from receiving probe to reconstruct the A-scan wave of the received signal, A-scan waveform is shown in Figure 3.

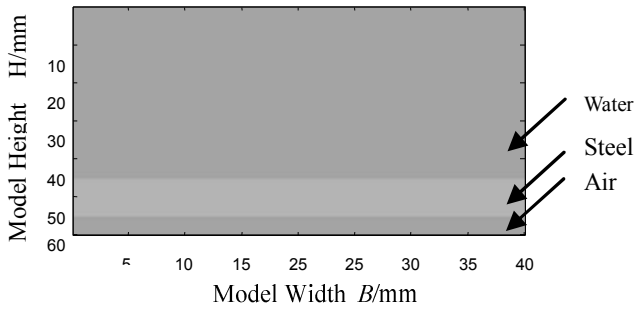

Fig. 1 The model of gas-liquid-solid coupling interface.

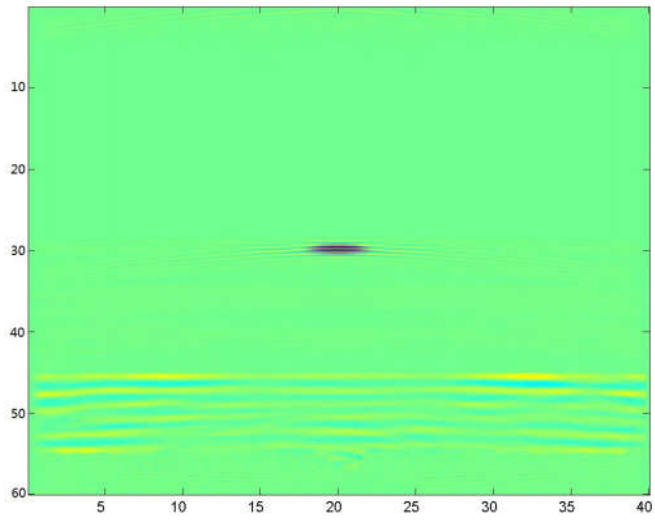

Fig. 2 Snapshot figure of the stress components under the boundary conditions of RIPML.

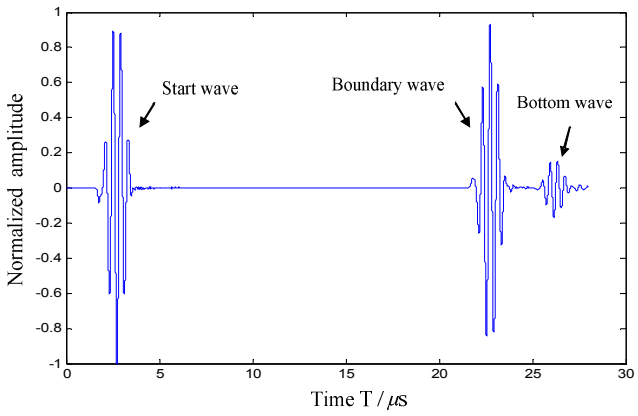

Fig. 3 A-scan waveform when no glitches.

IV. Numerical Analysis of the Inner Burr Ultrasonic Testing

A. Calculation Model

In the process of the inner burr removal, the main problems are scraping the partial, the amount of scraping is too large or too small, and remove of the inner burr is not clean and so on. According to the main types and characteristics of the inner burr, the simulation model of inner burr is designed. Calculation parameters of the ideal model, the width and height of burr are set respectively as $3mm$ and $2mm$. Different types of burrs are settled at the $16mm$ to $19mm$ of model width.

B. Analysis of inner burrs

The simulation calculation is based on the above three models. The probe move along the width direction, an A-scan result can be obtained at each interval of 0.25 mm. The normalized amplitude and normalized time of received echo are calculated according to the A-scan waveform data. The signal amplitude diagram of the bottom surface and a bottom thickness diagram are acquired with the moving of the probe, which is shown as Figure 5-7.

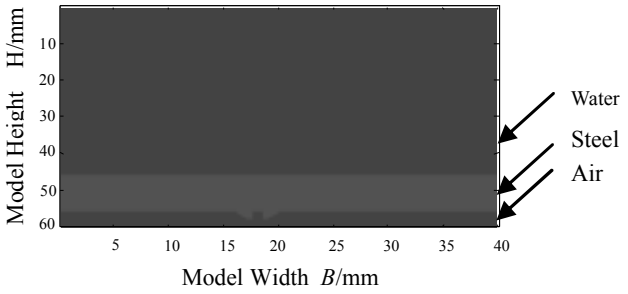

(a) Scraper blade deletion

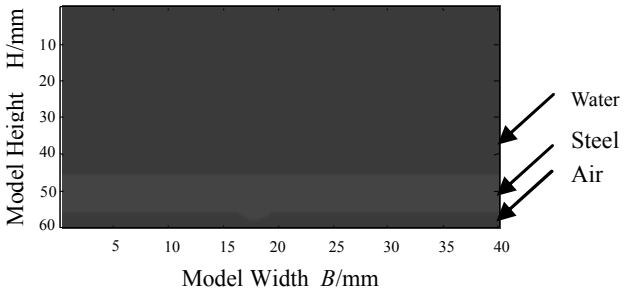

(b) The position of scraper is too high

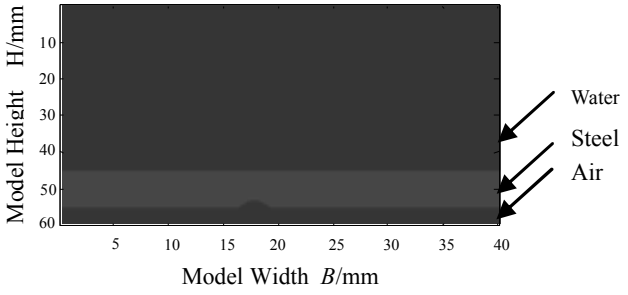

(c) The position of scraper is too low

Fig. 4 Calculation model of the inner burr.

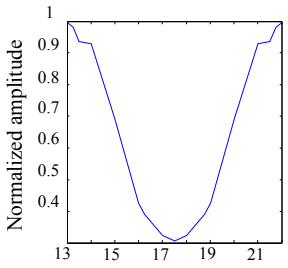

(a) Amplitude curve

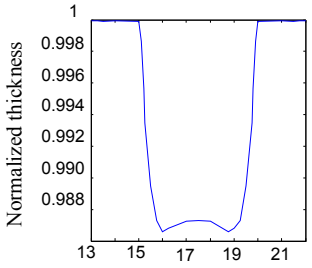

(b) Thickness curve

Fig. 5 Scraper blade deletion.

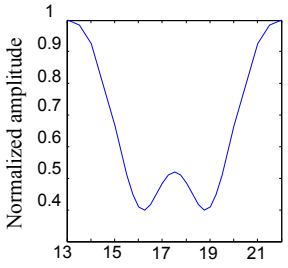

(a) Amplitude curve

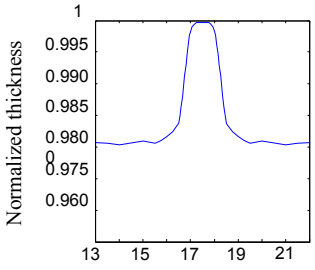

(b) Thickness curve

Fig. 6 The position of the scraper is too high.

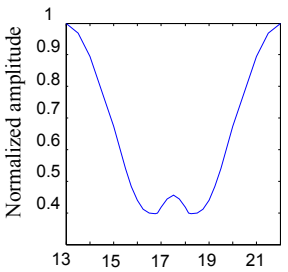

(a) Amplitude curve

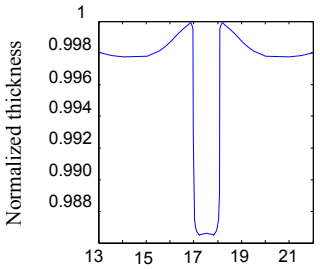

(b) Thickness curve

Fig. 7 The position of the scraper is too low.

The experiment results show that the received signal amplitude is sharp declined by the inner burr, while the information of the thickness is subject to change. Since the plane defect will cause the ultrasonic wave to reflect along one direction, the inclined surface of burrs can cause the probe also receive a portion of the reflected wave when the probe not vertical facing to the defect position. In addition, the amplitude of the received echo by probe sometimes enhanced due to the effect of the superposition.

As shown in Figure 7(b) and Figure 7(c), the echo amplitude at the top of burrs is bigger. From the perspective of echo time or thickness information, once burrs exist in the pipe, then the travel of ultrasonic waves will change, causing the peak time of the received echo to change. Then, burr types can be determined by comprehended the amplitude characteristics and thickness characteristics.

V. Experimental Results

Experimental system use the water immersion method to simulate site testing environment of the water-coupling, using line focused probe, diameter of the probe is $10mm$, and the center frequency is $5MHz$. Experimental device use the grating scale as the displacement transducer, and testing sample is an ERW welded steel pipe with $3mm$ thickness and $75mm$ diameter, the width of weld is $3mm$, the burr is the type of the position of scraper too high shown in Figure 8. Thickness curve of the welded pipe is shown in Figure 9.

Seen from the experimental results, the amplitude distribution is consistent with the calculation results. However, due to the weld of the experimental welded pipe were not treated, the inner surface is rough, and causing there is a large number of scattering noise in the bottom echo. In the received A-scan signal, the bottom echo signal amplitude in the weld is smaller due to be submerged with the noise signal, therefore, amplitude fluctuations within the scope of the weld is larger. Signal inhibition function is used to experiment results for comparison.

VI. Conclusion

(1) Finite Difference Time Domain method can be used easily in the simulation of ultrasonic propagation characteristics, providing a reference method for analysis and judgment to detect the inner burrs of welded pipe, algorithm architecture is simple and easy to implement.

(2) Recursive integration algorithm in the PML method is applied to absorb boundary in a two-dimensional sound field can reduce resource consumption and calculation, while having the same absorbing effect with a conventional split

PML method.

(3) Ultrasonic testing results of the inner burr have a significant change due to different types of burrs. Burr defects can be determined by a comprehensive analysis of their amplitude characteristics and thickness properties.

Fig. 8 Line focused ultrasonic probe and welded pipe.

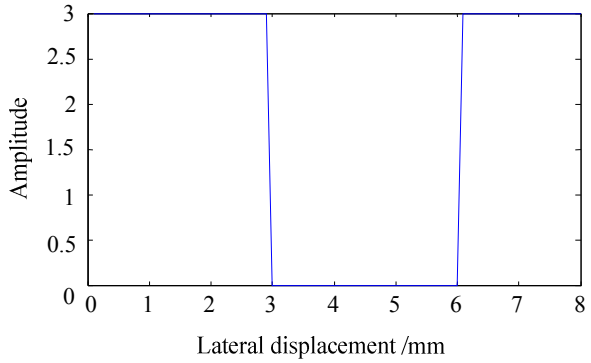

Fig. 9 Thickness amplitude curve.

REFERENCES

[1] D. P. Zhang, Z. J. Liu, and K. Zhao, "The common problems and solving methods for the inner burr of ERW welded pipe," *Chinese Welded Pipe and Tube*, vol. 31, no.5, pp. 73-95, 2008.

[2] Z. G. Zhou, and D. Wei, "Analysis of ultrasonic sound field characteristic with FDTD," *Chinese Journal of Mechanical Engineering*, vol. 49, no.2, pp. 9-15, 2010.

[3] J. P. Berenger, "A perfectly matched layer for the absorption of electromagnetic waves," *Journal Computation Physics*, vol. 114, no.2, pp. 185-200, 1994.

[4] M. N. Dmitriev, "Application of M-PML absorbing boundary condition to the numerical simulation of wave propagation in anisotropic media," *Numerical Analysis and Applications*, vol. 5, no.1, pp. 36-44, 2012.

[5] Y. T. Duan, B. Chen, H. L. Chen, and Y. T. Duan, "PML absorbing boundary condition for efficient 2-D WLP-FDTD method," *IEEE Antennas and Wireless Propagation Letters*," no.10, pp. 846-849, 2011.

[6] C. Marcinkovich, and K. Olsen, "On the implementation of perfectly matched layers in a three-dimensional fourth-order velocity-stress finite difference scheme," *Seg Technical Program Expanded Abstracts*, vol. 21, no.1, pp. 2027, 2002.

[7] C. Y Sun, and S. J. Li, "Wave equation numerical modeling by finite difference method with varying grid spacing," *Chinese Geophysical Prospecting for Petroleum*, vol. 47, no.2, pp. 123-127, 2008.

[8] D. Wei, and Z. G. Zhou, "Finite difference simulation of pulsed ultrasonic propagation in solid," *Chinese Acta Aeronautica Et Astronautica Sinica*, vol. 31, no.2, pp. 388-392, 2010.

[9] J. A. Roden, and S. D. Gedney, "Convolutional PML (CPML): an efficient FDTD implementation of the CFS-PML for arbitrary media," *Micro-wave and Optical Technology Letters*, no.27, pp. 334-339, 2000.

[10] M. Kuzuoglu, and R. Mittra, "Frequency dependence of the constitutive parameters of causal perfectly matched anisotropic absorbers," *IEEE Microwave and Guided Wave Letters*, vol. 6, no.12, pp.447-449, 1996.

[11] F. Collino, and C. Tsogka, "Application of the PML absorbing layer model to the linear elastodynamic problem in anisotropic media," *Geophysics*, vol. 66, no.1, pp. 294-307, 2001.

[12] K. Y. Chen, "Study on perfectly matched layer absorbing boundary condition," *Chinese Geophysical Prospecting for Petroleum*, vol. 49, no.5, pp. 472-477, 2010.

[13] G. Gao, and Z. H. He, "Analysis on attenuation factor in the processing of artificial boundary conditions of PML," *Chinese Geophysical Prospecting for Petroleum*, vol. 50, no.5, pp. 430-433, 2011.

[14] F. H. Drossaert, and A. A. Giannopoulos, "Nonsplit complex frequency-shifted PML based on recursive integration for FDTD modeling of elastic waves," *Geophysics*, vol. 72, no.2, pp. 9-17, 2007.

Dong Wei is with the School of Electronic and Information Engineering, University of Science and Technology Liaoning, Anshan, 114051, PR China. (phone: 86-0412-5929747; e-mail: asweidong@126.com).

Xue Zhao is a postgraduate student in the School of Electronic and Information Engineering, University of Science and Technology Liaoning, Anshan, 114051, PR China. (e-mail: zx992992@126.com).

Jing Wang is a postgraduate student in the School of Electronic and Information Engineering, University of Science and Technology Liaoning, Anshan, 114051, PR China. (e-mail: aswangjing@163.com).

Jie-sheng Wang received his B. Sc. And M. Sc. degrees in control science from University of Science and Technology Liaoning, China in 1999 and 2002, respectively, and his Ph. D. degree in control science from Dalian University of Technology, China in 2006. He is currently a professor and Master's Supervisor in School of Electronic and Information Engineering, University of Science and Technology Liaoning. His main research interest is modeling of complex industry process, intelligent control and Computer integrated manufacturing.